NASA Technical Memorandum 4335

# Failure Detection and Fault Management Techniques for a Pneumatic High-Angle-of-Attack Flush Airdata Sensing (HI-FADS) System

Stephen A. Whitmore and Timothy R. Moes

JANUARY 1992

NASA

NASA Technical Memorandum 4335

# Failure Detection and Fault Management Techniques for a Pneumatic High-Angle-of-Attack Flush Airdata Sensing (HI-FADS) System

Stephen A. Whitmore and Timothy R. Moes
*Dryden Flight Research Facility*
*Edwards, California*

National Aeronautics and
Space Administration

Office of Management

Scientific and Technical
Information Program

**1992**

# FAILURE DETECTION AND FAULT MANAGEMENT TECHNIQUES FOR FLUSH AIRDATA SENSING SYSTEMS

Stephen A. Whitmore* and Timothy R. Moes**
NASA Dryden Flight Research Facility
P.O. Box 273
Edwards, California 93523-0273

Cornelius T. Leondes†
University of Washington
FT 10, Electrical Engineering Department
Seattle, Washington 98195

## Abstract

A high-angle-of-attack flush airdata sensing system was installed and flight tested on the F-18 High Alpha Research Vehicle at the NASA Dryden Flight Research Facility. This system uses a matrix of pressure orifices arranged in concentric circles on the nose of the vehicle to determine angles of attack, angles of sideslip, dynamic pressure, and static pressure as well as other airdata parameters of interest. Results presented use an arrangement of 11 data ports distributed symmetrically on the aircraft nose.

Experience with this sensing system data indicates that the primary concern for real-time implementation is the detection and management of overall system and individual pressure sensor failures. The multiple port sensing system is more tolerant to small disturbances in the measured pressure data than conventional probe-based intrusive airdata systems. However, under adverse circumstances, large undetected failures in individual pressure ports can result in algorithm divergence and catastrophic failure of the entire system.

This paper demonstrates how system and individual port failures may be detected using $\chi^2$ analysis. Once identified, the effects of failures are eliminated using weighted least squares. Background on the HI-FADS hardware, the aerodynamic model, the nonlinear regression algorithm, and $\chi^2$ analysis are presented. Failure detection and fault management techniques are developed and data obtained from the High Alpha Research Vehicle flight tests are used to demonstrate the techniques.

## Nomenclature

| | |
|---|---|
| $A$ | angle-of-attack triples algorithm coefficient |
| $A'$ | angle-of-sideslip triples algorithm coefficient |
| $a$ | angle-of-sideslip triples algorithm coefficient |
| $B$ | angle-of-attack triples algorithm coefficient |
| $B'$ | angle-of-sideslip triples algorithm coefficient |
| $b$ | angle-of-sideslip triples algorithm coefficient |
| $C$ | angle-of-attack triples algorithm coefficient |
| $C'$ | angle-of-sideslip triples algorithm coefficient |
| DFRF | Dryden Flight Research Facility, Edwards, CA |
| DOF | degree of freedom |
| ESP | electronically scanned pressure |
| $F$ | aerodynamic model functional |
| FADS | flush airdata sensing system |
| $f$ | initialization algorithm coefficient function |
| HARV | High Alpha Research Vehicle |
| HI-FADS | High-Angle-of-Attack Flush Airdata Sensing |
| $i, j, k$ | indices |
| $M$ | Mach number |
| M | median HI-FADS residual magnitude |
| $Max[\,]$ | maximim value for vector [ ] |
| $N$ | number of HI-FADS pressure observations |
| NASP | National AeroSpace Plane |
| $P$ | HI-FADS pressure |
| $P_{max}$ | maximum allowable pressure for reason test |
| $P_{min}$ | minimum allowable pressure for reason test |
| $P_\infty$ | HI-FADS static pressure |
| $Prob()$ | probability of occurence |
| $Q_i$ | residual weighting |
| $q_c$ | HI-FADS compressible dynamic pressure |
| RT-FADS | real-time flush airdata sensing |
| $s$ | sample variance |
| $x$ | dummy variable of integration |

*Aerospace Engineer, member AIAA
**Aerospace Engineer
†Electrical Engineer, member AIAA

| | |
|---|---|
| $\alpha$ | angle of attack, deg |
| $\beta$ | angle of sideslip, deg |
| $\Gamma$ | Gamma function |
| $\gamma$ | probability distribution degrees of freedom |
| $\delta P$ | HI-FADS residual |
| $\varepsilon$ | HI-FADS calibration coefficient |
| $\theta$ | port incidence angle |
| $\lambda$ | HI-FADS cone angle |
| $\mu$ | residual mean |
| $\xi$ | number of parameters estimated from HI-FADS data |
| $\Sigma$ | summation operator |
| $\sigma\alpha$ | standard deviation of HI-FADS residuals |
| $\phi$ | high-angle-of-attack flush airdata sensing clock angle |
| $\chi^2$ | random variable distributed according to "chi-square" |
| $\hat{\chi}^2$ | estimate of chi-square variable |

## Introduction

Increasingly, flight system designs for advanced aerospace vehicles are requiring the availability of accurate and high-fidelity airdata values such as angle of attack ($\alpha$) and Mach number ($M$). For hypersonic vehicles like the National AeroSpace Plane (NASP), accurate airdata measurements are required for engine airframe integration. Because of the hostile hypersonic environment, conventional intrusive airdata systems would not survive on the NASP vehicle. For stealth vehicles such as the B-2 flying wing, direct feedback from the airdata system is used for vehicle control. Again, because of low observability requirements, conventional intrusive airdata measurement systems cannot be used. For high-angle-of-attack vehicles, a conventional noseboom installation would alter the basic flow characteristics of the aircraft nose and may adversely affect aircraft performance. As a means of circumventing these difficulties, the flush airdata sensing (FADS) system concept was originated at the NASA Langley Research Center and developed and flight tested at the NASA Dryden Flight Research Facility (DFRF).

Several FADS demonstration programs have been performed. Early programs conducted on the KC-135 and F-14 vehicles were intended only to demonstrate the feasibility of the concept and did not attempt to derive algorithms capable of operating on a fully redundant flight system.[1,2] Instead, the emphasis of these flight programs was on measurement and presentation of individual pressure coefficient data and their empirical relationships to Mach number, dynamic pressure, and flow incidence angles. The shuttle entry airdata sensing (SEADS) system demonstrated the feasibility of the FADS concept at hypersonic speeds.[3]

A more advanced program demonstrated the feasibility of using a high-angle-of-attack flush airdata sensing (HI-FADS) system for research flight measurements. This program concluded during phase 1 of the F-18 High Alpha Research Vehicle (HARV) flight tests at NASA DFRF. The HI-FADS design is an evolution of the earlier nonintrusive systems and emphasized the airdata algorithm development with composite results expressed as airdata estimates instead of raw pressure values. The HI-FADS system provided the opportunity to research various application techniques for FADS as vehicle or mission-critical flight systems. The HI-FADS system incorporated an overdetermined algorithm in which surface pressure observations operated simultaneously to infer the airdata parameters using nonlinear regression. Excellent results were achieved for flights conditions up to $\alpha = 55$ and $M = 1.20$. Standard errors were empirically determined to be approximately one-half degree in angle of attack and angle of sideslip, and better than 0.004 in Mach number. References 4, 5, and 6 contain preliminary results of these flight tests.

The nonlinear regression algorithm from phase 1 of the HARV flight tests was shown to be insensitive to small disturbances in the measured pressures, but because of the nonlinearity of the HI-FADS model, the algorithm is not robust to large sensor errors. For example, these errors are caused by failed sensors and blocked ports. Divergence and complete system failure may occur if large errors are input to the algorithm without using divergence protection and regression. Thus, a primary concern for real-time implementation is failure detection and fault management of sensor failures.

For the algorithm to be divergence-safe, a criterion for identifying system failure and imminent algorithm divergence must be developed. Using this criterion, failed pressure observations can be weighted out of the algorithm before divergence becomes a problem. Studies on the HARV HI-FADS data indicate that using the regression algorithm bad observations are weighted out of the algorithm, good airdata results can be achieved with as little as seven observations. Thus, for sensing systems with more than seven sensors, one or more failures can be tolerated at a given data frame.

This paper demonstrates how total system and individual measurement failures can be identified using $\chi^2$ analysis of the pressure measurement residuals. Techniques for making the algorithm tolerant to pressure sensor failures using weighted least squares will be developed. Background on the HI-FADS systems, nonlinear regression, and $\chi^2$ analysis will be presented. Data derived from HI-FADS flight tests will be used to demonstrate the concepts presented and methods developed.

The failure detection and fault management techniques were developed to support the immediate needs of a real-time flush airdata sensing (RT-FADS) system. This flight-test demonstration program is in the planning stages and is a

collaborative effort between NASA DFRF, McDonnell Aircraft (McAir, St. Louis, Missouri), and Honeywell Inc. (St. Louis Park, Minnesota). The effort seeks to demonstrate in real time the capabilities of a FADS system onboard the DFRF Systems Research Aircraft (SRA), a 2-seat FA-18b. The RT-FADS system is based on the HI-FADS architecture, but airdata computations will be performed in onboard precessors. The evaluated airdata will be displayed to the pilot and telemetered to ground in real time.

## High-Angle-of-Attack Flush Airdata Sensing System

### Hardware

The HI-FADS configuration has a simple hardware arrangement with the basic fixture being a fiberglass reinforced plastic cap mounted on the nose of the F-18 HARV. Twenty five 0.06-in. diameter pressure orifices arranged in 4 annular rings were drilled in the nosecap. Flight tests conducted during phase 1 of the HARV program indicated that airdata could be satisfactorily measured using a subset of the 25 pressure ports. All results presented in this paper use 11 ports symmetrically distributed about the nosecap. Early HI-FADS flight tests indicated that satisfactory airdata results can be achieved using as little as 7 pressure measurements, therefore, this formulation used 11 ports to allow for up to 4 pressure failures at any given data frame. Quad-redundancy (in terms of pressure measurements) is thus achieved.

The locations of the nosecap ports were defined using clock and cone angle coordinates measured relative to the nosecap axis of symmetry. The cone angle ($\lambda$) is the total angle that the normal to the surface makes with respect to the nosecap axis of symmetry. The clock angle ($\phi$) is the clockwise angle looking aft around the axis of symmetry starting at the bottom of the fuselage. Figure 1 illustrates the definitions of the clock and cone angles as well as the pressure ports locations. Table 1 lists the coordinate angles of the various pressure ports used in the 11-port analysis.

Table 1 HI-FADS pressure port locations

| Port # | Clock angle, deg | Cone angle, deg |
|---|---|---|
| 1 | 0.0 | 0.0 |
| 2 | 0.0 | 20.0 |
| 3 | 180.0 | 20.0 |
| 4 | 0.0 | 55.0 |
| 5 | 90.0 | 55.0 |
| 6 | 180.0 | 55.0 |
| 7 | 270.0 | 55.0 |
| 8 | 45.0 | 60.0 |
| 9 | 135.0 | 60.0 |
| 10 | 225.0 | 60.0 |
| 11 | 315.0 | 60.0 |

Pressures at the nosecap were sensed by a multiple transducer, electronically scanned pressure (ESP) module, remotely mounted in the aircraft nose cavity. Pressures at the surface were transported to the ESP module using lengths of flexible pneumatic tubing. Analyses performed in reference 6 indicate that the pneumatic tubing did not introduce any significant distortions in the measured pressure values in the bandwith of interest (0-20 Hz). The ESP module, which consists of differential transducers, was referenced to a single, high-accuracy absolute pressure transducer mounted in the aircraft nose cavity. High-frequency dynamics in the reference pressure were attenuated by a damping tank also mounted in the aircraft nose. The temperature environments of both the ESP module and the reference transducer were controlled by wrapping the units in heater blankets to maintain a constant operating temperature. All HI-FADS pressure data were digitally encoded onboard using a 10-bit pulse code modulation (PCM) system and telemetered to ground where selected pressures were displayed in real time. All HI-FADS data were recorded at 25 samples/sec. for postflight analysis. More detail concerning the HARV flight-test program and HI-FADS system hardware may be found in Ref. 4, 5, 6, and 7. A schematic of the HARV HI-FADS system is shown in Fig. 2.

### Aerodynamic Model

Measured pressure data are related to airdata state parameters by way of a nonlinear aerodynamic model derived from potential flow in reference 4. The model prescribes measured pressure in terms of four airdata parameters: dynamic pressure ($q_c$), angle of attack ($\alpha$), angle of sideslip ($\beta$), and static pressure ($P_\infty$). Using these four basic airdata parameters, most airdata quantities of interest may be directly calculated. For a given pressure observation

$$P(\phi_i, \lambda_i) = q_c \left[\cos^2(\theta_i) + \varepsilon \sin^2(\theta_i)\right] + P_\infty \qquad (1)$$

where $\phi_i$ and $\lambda_i$ are the clock and cone angles of the i'th pressure port, $\varepsilon$ is a calibration parameter which varies as a function of $M$ and $\alpha$, and $\theta_i$ is the incidence angle between the surface and the velocity vector. The incidence angle is related to the local $\alpha$ and $\beta$ by

$$\begin{aligned}\cos(\theta_i) = {} & \cos(\alpha)\cos(\beta)\cos(\lambda_i) \\ & + \sin(\beta)\sin(\phi_i)\sin(\lambda_i) \\ & + \sin(\alpha)\cos(\beta)\cos(\phi_i)\sin(\lambda_i)\end{aligned} \qquad (2)$$

Here $\alpha$ and $\beta$ are not corrected for aircraft induced upwash and sidewash. As with conventional intrusive airdata sensors, independent calibration must be done for the aircraft induced measurement errors. Techniques for calibration of the indicated $\alpha$ and $\beta$ are described in detail in Ref. 4.

### Nonlinear Regression Algorithm

Although the pressure model is accurate in relating the airdata parameters to the measured pressure data, it is nonlinear and cannot be directly inverted to give airdata as a

function of the measured pressures. Instead, for each data frame, the pressure measurements are used as indirect observations and the airdata parameters are estimated using a weighted nonlinear least-squares regression. Within each frame, the algorithm is linearized about a starting value and all pressure data are used simultaneously to evaluate the least- squares perturbations about the starting value. Within each frame, the algorithm is iterated until convergence. At the beginning of each new data frame the system is relinearized about the result of the previous frame, and the iteration is repeated using new pressure data, thus the algorithm is time-recursive as well as iterative. This recursive, iterative, and overdetermined (more observations than states) structure makes the algorithm stable and robust to small perturbations in the measured pressure data.

### Algorithm Divergence

Difficulty with the nonlinear regression algorithm occurs when a large disturbance such as a data spike or bit-dropout occurs in a measured pressure value. Recall that the HI-FADS algorithm is nonlinear; consequently, one true minimum and multiple false minima will exist. If a large disturbance is undetected and not weighted out of the regression, the resulting state perturbation may dump the algorithm into a node which converges to a false minimum. At this point the algorithm will compute nonsensical results or may diverge altogether. In any case, once a false minimum has been reached, the algorithm will not reliably be able to return to the true minimum without reinitializing the algorithm with a new starting condition.

Figure 3 presents a one-dimensional illustration of the relationship between false minima and algorithm divergence. In Fig. 3, the marker indicates the value of the least-squares cost index (the sum of the squares of the residuals) for a given value of the state estimate. When the marker lies at 1, the algorithm is nondivergent but still needs additional iterations before convergence is reached. When the marker lies at 2, the algorithm has reached the global minimum and has converged. If a large pressure deviation were to occur, the algorithm could be dumped into a false node, (marker 3), and converge to a false minimum which returns a nonsensical answer, (marker at 4).

### Algorithm Initialization

For the regression algorithm to begin computations, a reasonable initial estimate of the airdata parameters must be available. For the HI-FADS algorithm, this initial estimate is provided by strategic manipulation of pressure "triples," which allow the $\alpha$ and $\beta$ to be explicitly solved for. This computation, referred to as the "triples" algorithm, tends to be noisy and not as robust to data perturbations as the HI-FADS algorithm; however, it allows a direct computation of the airdata using only measured pressures and does not require a starting value. If $\theta$ is evaluated using the triples values for $\alpha$ and $\beta$, Eq. (1) can be expressed as a linear equation in terms of $q_c$ and $p_\infty$, and least-squares solutions for $q_c$ and $p_\infty$ can be written in closed form.

The starting airdata parameters are evaluated each time the algorithm is initialized and the algorithm is iterated to convergence (typically 4-5 iterations). Once initial convergence is reached, the triples algorithm is no longer used and the HI-FADS algorithm is operated in the recursive–iterative mode as discussed earlier. A complete derivation of the triples algorithm is presented in the appendix.

## Methods of $\chi^2$ Analysis

This section presents a brief review of the methods of $\chi^2$ analysis, as the failure detection method to be developed is based on the $\chi^2$ goodness-of-fit test. If a sample of $N$ independent random data values is taken from a Gaussian distributed population with zero mean and unit variance, then the sum of the squares of those numbers is distributed according to the so-called "chi-squared" distribution.[8,9]

$$Prob(\chi^2) = \int_0^{\chi^2} \frac{\left(-\frac{1}{2}x\right)^{\frac{\gamma-2}{2}}}{2^{\gamma/2}\Gamma(\gamma/2)} e^{-\frac{1}{2}x} dx \qquad (3)$$

where $\gamma = N-1$ degrees-of-freedom (DOF) for the distribution. $\Gamma(\gamma/2)$ is the gamma function evaluated at one-half of the DOF.

In a Gaussian distributed population of random numbers with mean $\mu$, and variance $\sigma^2$, if the sample variance, estimated by

$$s^2 = \sum_1^N \frac{(x-\mu)^2}{N-1}$$

is normalized by multiplying by

$$\frac{(N-1)}{\sigma^2}$$

then resulting ratio

$$\chi^2 = \frac{(N-1)}{\sigma^2} s^2 \qquad (4)$$

is a random number distributed according to $\chi^2$. For numbers selected from a completely independent population, the $\chi^2$ parameter will have $N-1$ DOF. If the members of the population are related by $\xi$ parameters which have been estimated from the data, the DOF is reduced by $\xi$, i.e., $\gamma = N - \xi - 1$.

Thus, if a small subset is taken randomly from a Gaussian-distributed population whose mean and variance are known, and the sample variance is evaluated for that subset, then the odds of randomly selecting that subset are readily evaluated using the $\chi^2$ distribution. As demonstrated in the following HI-FADS Failure Detection and Fault Management Techniques section, this feature is particularly useful in least-squares problems for evaluating the accuracy of curve-fits. The $\chi^2$ test is completely reliable and for small sample populations, statisticians regard this test as the singularly most reliable goodness-of-fit test available.[8,9]

## High-Angle-of-Attack Flush Airdata Sensing Failure Detection and Fault Management

At the beginning of each iteration, the HI-FADS algorithm linearizes the aerodynamic model about the result from the previous iteration. The first step of this linearization is the evaluation of the residuals between the measured pressure data, and the HI-FADS model predictions for each port

$$\delta P_i^{j+1} = P_i - F^j(\alpha, \beta, q_\infty, P_\infty, \lambda_i, \phi_i, \varepsilon), i = 1, \ldots N \quad (5)$$

Here, $i$ is the port index and $j$ is the iteration index. These residuals are observations from which the least-squares regression algorithm estimates the optimal perturbations to the state parameters.

For a given data frame, the HI-FADS residuals represent a small subset of a larger random population. The statistical properties of this population may be empirically evaluated using large samples of converged airdata. If a smoothed histogram of the residuals (divided by dynamic pressure to scale the magnitudes) for a large data set is evaluated, the result is a family of approximately zero-mean, Gaussian probability density curves. The variances of these curves are proportional to angle of attack. These density curves are computed empirically using nonfailed HI-FADS flight data. Figure 4 shows the sample variances plotted as a function of angle of attack for this family of curves. These sample variances, evaluated using nearly a half-million data frames from multiple flights, represent the true population statistics. Data in which visual inspection determined that the airdata computations were not converged were excluded from this sample set. If the individual distributions for the various angle of attack regions are normalized by the sample-variance values taken from Fig. 4, then the distributions reduce to a single probability density curve very close to the standard zero-mean, unity-variance Gaussian probability density curve. This comparison is presented in Fig. 5.

Figure 5 gives clear evidence that the individual residuals are Gaussian distributed. Therefore, for a given data frame, the sum-square of the scaled-residuals (divided by the variance) should be distributed as a $\chi^2$ variable with $N - 6$ DOF. The DOF are reduced by 5 because the residuals are related by 5 parameters which have been computed from them. These parameters are the airdata states, $q_c$, $\alpha$, $\beta$, and $P_\infty$, and the calibration parameter, $\varepsilon$. For the case of 11 ports, this would give a distribution with 5 DOF. The HI-FADs residuals behave according to this distribution. This is verified by evaluating

$$\hat{\chi}^2 = \sum_{i=1}^{N} \frac{\left[\frac{\delta P_i}{q_c}\right]^2}{\sigma_\alpha^2} \quad (6)$$

at the beginning of each iteration, and plotting a large sample histogram of the resulting values. In Eq. (6), the variance, $\sigma_\alpha^2$, is evaluated using the data of Fig. 4. The $\hat{\chi}^2$ histogram data are presented in Fig. 6. The theoretical and empirical density functions are in close agreement.

The residual statistics were evaluated using only converged airdata values. Evaluating $\hat{\chi}^2$ at the beginning of an algorithm iteration allows the hypothesis for airdata failure to be observed by comparing the value of $\hat{\chi}^2$ against percentage points of $\chi^2$ distribution taken from

$$1 - Prob(\hat{\chi}^2) = \int_{\hat{\chi}^2}^{\infty} \frac{\left(-\frac{1}{2}x\right)^{\frac{\gamma-2}{2}}}{2^{\gamma/2}\Gamma(\gamma/2)} e^{-\frac{1}{2}x} dx \quad (7)$$

The probability of a given value of $\hat{\chi}^2$ occurring without airdata failure is given by Eq. (7). Since $\hat{\chi}^2$ is a relative probability indicator depending upon the value of $\hat{\chi}^2$, various failure detection modes can be initiated. The HI-FADS flight data indicate that for a small value of $\hat{\chi}^2$, the algorithm is near convergence and usually only one additional iteration is necessary. An intermediate value indicates that although the incoming pressure data is of reasonable quality, further iterations are likely required to reach convergence. A large value of $\hat{\chi}^2$ indicates a high probability that some system failure has occurred and tests on individual pressure data should be performed.

Based on the relative probability properties of the $\chi^2$ distribution, the HI-FADS algorithm operates in three basic modes. These modes are nominal; in which only one iteration is performed at each data frame; iteration; in which multiple iterations are required to reach convergence; and fault management, in which individual pressure failures are detected and weighted out of the regression. Figure 7(a) is a schematic of the algorithm structure and the transitions between the various algorithm modes. Each of the algorithm modes is discussed in detail.

### Nominal Mode

If Eq. (7) is evaluated for $\hat{\chi}^2 = 1.61$, a 90-percent (5 DOF) probability results and indicates a significant likelihood that no airdata failure has occurred. In fact, experience with HI-FADS data indicates that for low values of $\hat{\chi}^2$ the algorithm is near convergence and only one iteration for each data frame is necessary. This one iteration per data frame is the nominal mode for the algorithm and corresponds to the location of marker 2 in Fig. 3. The nominal mode is the regular operation mode of the algorithm and allows the fastest data throughput. For a 5-DOF system, the nominal mode is implemented as long as $\hat{\chi}^2 < 4.35$. The algorithm drops out of the nominal mode only at high-angles of attack, during highly dynamic flight conditions, or when data channel failures occur.

### Iteration Mode

A $\hat{\chi}^2$ value of 4.35 corresponds to a probability of approximately 50 percent, and indicates an equal probability of algorithm convergence or nonconvergence. Experience with the HI-FADS data indicates that for intermediate values of $\hat{\chi}^2$, no airdata failure has occurred. However, several

iterations may be required to reach the convergence point. In this regard, the $\hat{\chi}^2$ value provides a solid convergence criterion. This is the iteration mode for the algorithm and it corresponds to the location of marker 1 in Fig. 3. The iteration mode is usually entered at high-angles of attack or loaded maneuvering and is somewhat slower than the nominal mode. For the 5-DOF system, the iteration mode is implemented when $4.35 \leq \hat{\chi}^2 < 15.1$.

**Fault Management Mode**

A $\hat{\chi}^2$ of 15.1 corresponds to a probability of 1 percent and indicates a high probability of failure in the airdata system. In this case, some individual channel failure detection and fault management must be implemented to keep the algorithm from diverging. This is the fault management mode of the algorithm. The fault management mode corresponds to the location of marker 3 in Fig. 3. The throughput of the fault management mode is reduced considerably because testing on individual pressure values is required for each failed data frame. For the 5-DOF system, the fault management mode is implemented when $15.1 \leq \hat{\chi}^2$.

**Fault Management Tests**

This section defines the fault management tests implemented when the system has failed the $\chi^2$ test (and the fault management mode is entered). The $\chi^2$ method allows nominal algorithm operation with little overhead for fault-detection and serves as an indicator of the overall system health. Failure tests on individual ports need to be performed only when a $\chi^2$ test failure has occurred. A series of tests are performed when $\chi^2$ failures occur, ranging from simple to complex and computationally intensive. For the HI-FADS algorithm, four tests for individual port failures have been implemented. Figure 7(b) is a detail of the fault management mode and depicts the transitions between the various port-failure tests.

The first fault management test is a simple reason check. Upon failure of the $\chi^2$ test ($\hat{\chi}^2 > 15.1$ for 5-DOF), the weight of any pressure data value which is less than a specified minimum or greater than a specified maximum is set to zero. Data values which lie between the specified minimum and maximum values are given a weight of 1. The weighted $\hat{\chi}^2$ is reevaluated using the new weights

$$\hat{\chi}^2 = \sum_{i=1}^{N} Q_i \frac{\left[\frac{\delta P_i}{q_c}\right]^2}{\sigma_\alpha^2} \tag{8}$$

and the result is compared against the percentage points of $\chi^2$ distribution for

$$\gamma = \sum_{i=1}^{N} Q_i - 6$$

DOF. If the corresponding probability percentage is greater than or equal to 1 percent (the probability at which the fault management mode is entered) and $\gamma > 0.0$, the algorithm drops out of the failure testing mode and enters the iteration mode using the newly assigned weights.

If after the reason test has been implemented, $Prob(\hat{\chi}^2) < 1$ percent or $\gamma \leq 0.0$, then the next failure detection test is performed, a simple three-sigma residual test where the weights are reassigned based on residual magnitudes. For each of the data channels, if $\delta p_i/q_c < \sigma_\alpha$, then $Q_i = 1.0$. If $\sigma_\alpha < \delta p/q_c < 3\sigma_\alpha$, then the weight for that residual is set to

$$Q_i = -\frac{1}{2}\left\{\frac{\left[\frac{\delta P_i}{q_c}\right]^2}{\sigma_\alpha^2}\right\} + \frac{3}{2},$$

for $3\sigma_\alpha < \delta p/q_c$ the weight is set to zero. After reevaluating the weights, the weighted $\hat{\chi}^2$ value is evaluated again and compared against percentage points of $\chi^2$ distribution for

$$\gamma = \sum_{i=1}^{N} Q_i - 6$$

DOF. If the resulting $Prob(\hat{\chi}^2) \geq 1$ percent and $\gamma > 0.0$, the algorithm drops out of the failure testing mode and enters the iteration mode using the newly assigned weights. For this test in which fractional weights are allowable, non-integer values for the DOF are possible.

If after the 3-$\sigma$ test has been implemented, $Prob(\hat{\chi}^2) < 1$ percent or $\gamma \leq 0.0$, then the next failure detection test is used. The third test, for measurement consistency, is more computationally intensive than are the two previous tests and is intended as a catch-all test. Consistency refers to equality of the residual magnitudes. For this test, the weight of the residual with the magnitude farthest from the median residual magnitude is set to zero. All other weights are set to 1. The weighted value of $\hat{\chi}^2$ is evaluated and the result is compared against $Prob(\hat{\chi}^2)$ for $N - 7$ DOF. If $Prob(\hat{\chi}^2) \geq 1$ percent, the algorithm drops out of the failure testing mode and enters the iteration mode using the newly assigned weights. If $Prob(\chi^2) < 1$ percent, then the weight of the residual in which the magnitude is next farthest from the median is set to zero. The weighted value of $\hat{\chi}^2$ is again computed and the results are compared against $Prob(\hat{\chi}^2)$ for $N - 8$ DOF. Again if $Prob(\hat{\chi}^2) \geq 1$ percent, the algorithm drops out of the testing loop; otherwise, the process is repeated again until $\gamma \leq 0$.

If $\gamma \leq 0$ at the end of the consistency test cycle, then either the hold-last-value or reset sub-modes will be entered. The hold-last-value sub-mode is entered first. In this mode, the least-squares regression is bypassed and the value of the airdata state remains unchanged. After skipping the regression, all of the weights are set to 1.0, the hold index (which indicates the number of consecutive holds) is incremented, and the algorithm returns to the nominal mode for the next data frame. The hold-last-value sub-mode allows small sections of corrupt input data to be passed over without triggering algorithm divergence or nuisance resets.

If the hold-last-value mode has been entered for a specified number (default 20) of consecutive data frames, then the algorithm has likely diverged or converged to a false solution, and the reset sub-mode is entered. This condition corresponds to the location of marker 4 in Fig. 3. In this case, the residuals are so far from the true minimal values that the algorithm must be reinitialized using a new set of starting values. Rough airdata estimates are evaluated using the triples algorithm discussed earlier. After the algorithm is relinearized about the starting values, it is iterated to convergence. When convergence is reached, all weights are set to 1.0, the hold index is set to zero, and the nominal mode is entered.

## Application to High-Angle-of-Attack Flush Airdata Sensing Flight Data

Figures 8(a) and 8(b) show applications of the failure detection and fault management techniques using F-18 HARV flight data. In the first case, the incoming pressures experience a series of large magnitude data spikes which cause catastrophic algorithm failure. In the second case, the data from several pressure channels experienced data steps caused by a malfunction of an experimental signal conditioning circuit designed to zero out the DC-level reading of the pressure transducers. These steps cause the algorithm to converge to a false solution.

Figure 8(a) shows the measured pressure data. When the data spikes are run unprotected through the FADS algorithm, catastrophic divergence results. Results from the diverged algorithm are presented in Fig. 8(b) where the computed angle-of-attack time history is plotted. Although the data values prior to divergence are valid, their values are not distinguishable in this figure. In Fig. 8(c), the pressure data along with the HI-FADS curve fit are plotted against incidence angle ($\theta$). The curve fit has little relationship to the ESP data and the large residuals (the distances from the curve fit to the ESP data) are indicative of algorithm divergence. Clearly the diverged airdata estimates are meaningless and this fact is reflected by the excessively large $\hat{\chi}^2$ value. For the diverged data, the $\hat{\chi}^2$ time history is presented in Fig. 8(d). After the first data spike, $\hat{\chi}^2$ assumes very large values, indicating catastrophic divergence.

When the $\chi^2$ criterion is used to test for algorithm divergence and the fault management mode is evoked, the algorithm behaves as intended. For the first example, the incoming data spikes tripped the reason limits. The corresponding weights of the pressure values exceeding these limits were set to zero. The resulting computed angle-of-attack time history is presented in Fig. 8(e). In Fig. 8(f), the pressure data and the HI-FADS curve fit are plotted against $\theta$. The curve fit neatly matches the measured data. The small residuals are indicative of algorithm convergence and this is reflected by the small $\hat{\chi}^2$ value. For the divergence protected algorithm, the computed $\hat{\chi}^2$ time history is presented in Fig. 8(g). Only at the points of the spikes does the $\hat{\chi}^2$ value become large and cause the fault management mode to trigger.

In the second example, the signal conditioning circuit introduced small but significant steps in the incoming pressure data. The corrupted pressure data time histories are presented in Fig. 9(a). If the corrupted data are passed to the HI-FADS algorithm unprotected, the algorithm converges to an erroneous solution and does not return. The angle-of-attack time history is presented in Fig. 9(b). In contrast to the earlier case, when the fault management mode is evoked, the bit-dropout residuals do not violate the reason limits and must rely on the 3-$\sigma$ criterion to detect the failure. In this case, the relative weighting scheme is initiated to protect the algorithm against divergence. The resulting angle-of-attack output is presented in Fig. 9(c). Here the algorithm converges and proceeds as normal, with the effects of the data dropout being indistinguishable. The computed $\chi^2$ time history is presented in Fig. 9(d). At the $\chi^2$ large values, a $\chi^2$ test failure was triggered and the fault management mode was initiated. The method clearly worked as expected.

No actual data failures which required the algorithm to enter the consistency tests or trip the hold-last-value or reset sub-modes were experienced during the HI-FADS flight tests. The validity of these sub-modes was verified through extensive simulation. Results of this validation and verification effort are beyond the scope of this paper and will not be presented.

## Summary and Concluding Remarks

A prototype nonintrusive airdata system was installed and flight tested on the F-18 High Alpha Research Flight Vehicle at the NASA Dryden Flight Research Facility. This system used a matrix of pressure orifices arranged in concentric circles on the nose of the vehicle to estimate the airdata parameters angle of attack, angle of sideslip, dynamic pressure, and static pressure. The high-angle-of-attack flush airdata sensing system hardware and regression algorithm were discussed.

Results indicated that if a large disturbance in a measured pressure value passed undetected into the HI-FADS algorithm, the resulting state perturbation could dump the algorithm into a false minimum and result in algorithm divergence or convergence to a false answer. The need for algorithm protection was discussed. Failure detection and fault management techniques based on $\chi^2$ analysis and weighted least squares were developed. This paper demonstrated how system and individual port failures may be detected using $\chi^2$ analysis. Once identified, the effects of failures are eliminated using weighted least squares. Data obtained from the High Alpha Research Vehicle flight tests were used to demonstrate the techniques.

Use of the developed failure detection and fault management techniques allow a single pressure measurement matrix to be multiply redundant. As illustrated with flight data,

the $\chi^2$ method allows several of the pressure measurements to fail simultaneously with little or no degradation of the resulting airdata computations The utility of the $\chi^2$ method as an indicator of the overall system health is that it requires little overhead for fault detection. Failure tests on individual ports need to be performed only when a $\chi^2$ test failure has occurred. This allows the algorithm to operate in a nominal mode in which only one iteration and no individual pressure failure checking is required. This provides a much greater computational throughput than would be possible if multiple iterations and individual pressure checking were required at each data frame. The increased throughput will be valuable for feedback systems in which the maximum available airdata rate is desired.

## References


[1] Larson, Terry J. and Paul M. Siemers, III, *Use of Nose Cap and Fuselage Pressure Orifices for Determination of Air Data for Space Shuttle Orbiter Below Supersonic Speeds*, NASA TP-1643, 1980.

[2] Larson, Terry J., Stephen A. Whitmore, L. J. Ehernberger, J. Blair Johnson, and Paul M. Siemers, III, *Qualitative Evaluation of a Flush Airdata System at Transonic Speeds and High Angles of Attack*, NASA TP-2716, 1987.

[3] Siemers, Paul M., III, Henry Wolf, and Martin W. Henry, *Shuttle Entry Air Data System (SEADS)-Flight Verification of an Advanced Air Data System Concept*, AIAA 88-2104, 1988.

[4] Whitmore, Stephen A., Timothy R. Moes, and Terry J. Larson, *Preliminary Results From a Subsonic High Angle-of-Attack Flush Air Data Sensing (HI-FADS) System: Design, Calibration, and Flight Test Evaluation*, NASA TM-101713, 1990.

[5] Moes, Timothy R. and Stephen A. Whitmore, *Preliminary Results From an Airdata Enhancement Algorithm with Application to High Angle-of-Attack Flight*, NASA TM-101737, 1991. See also AIAA 91-0672, 1991.

[6] Whitmore, Stephen A. and Timothy R. Moes, *The Effects of Pressure Sensor Acoustics on Airdata Derived From a High-Angle-of-Attack Flush Airdata Sensing (HI-FADS) System*, AIAA 91-0671, 1991.

[7] Schneider, Edward T. and Robert R. Meyer, Jr., *F-18 High Alpha Research Vehicle Description, Results, and Plans*, Society of Experimental Test Pilots (SETP), 1989 Report to the Aerospace Profession, Proceedings, 1989, pp. 135-162.

[8] Bendat, Julius S. and Allan G. Piersol, *Random Data: Analysis and Measurement Procedures*, John Wiley & Sons, Wiley-Interscience, New York, 1971.

[9] Freiberger, W. F., ed., *The International Dictionary of Applied Mathematics*, D. Van Nostrand Co., Inc, Princeton, New Jersey, 1960.


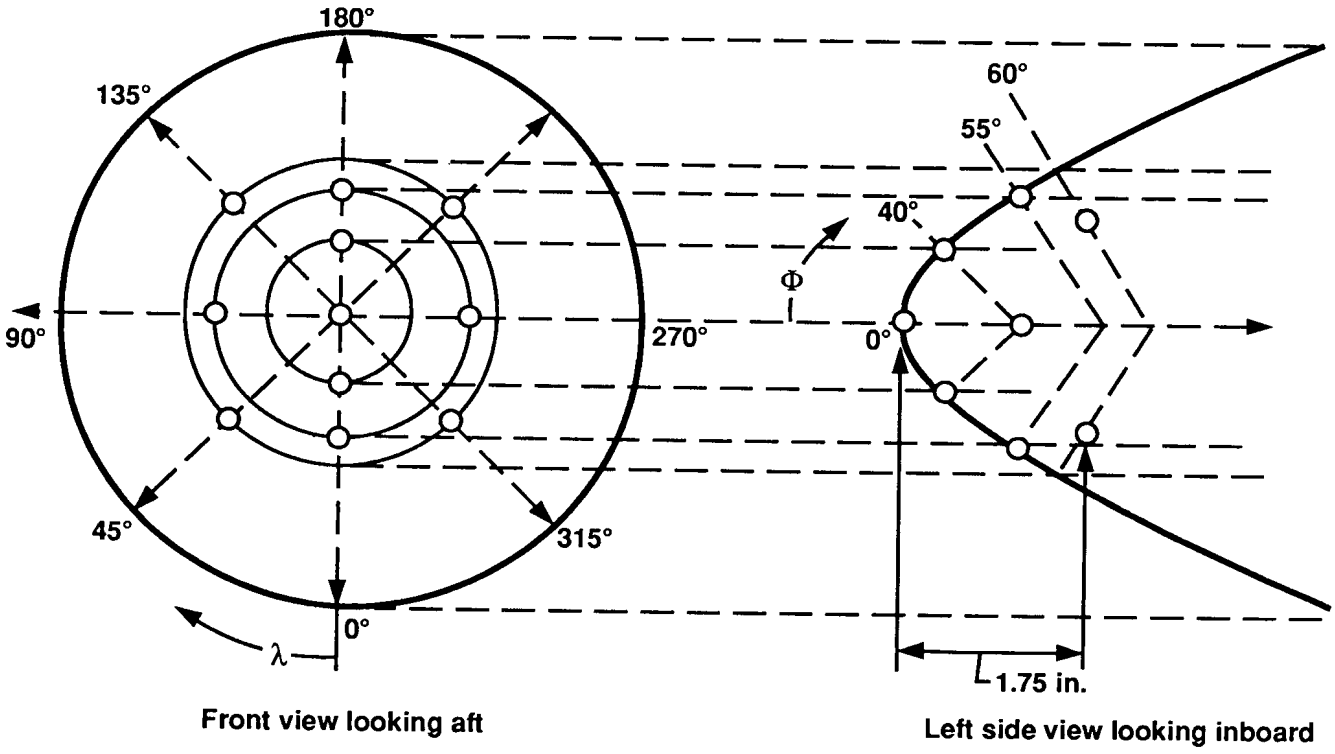


Figure 1. Scematic of HI-FADS nosecap showing coordinate definitions and port locations.

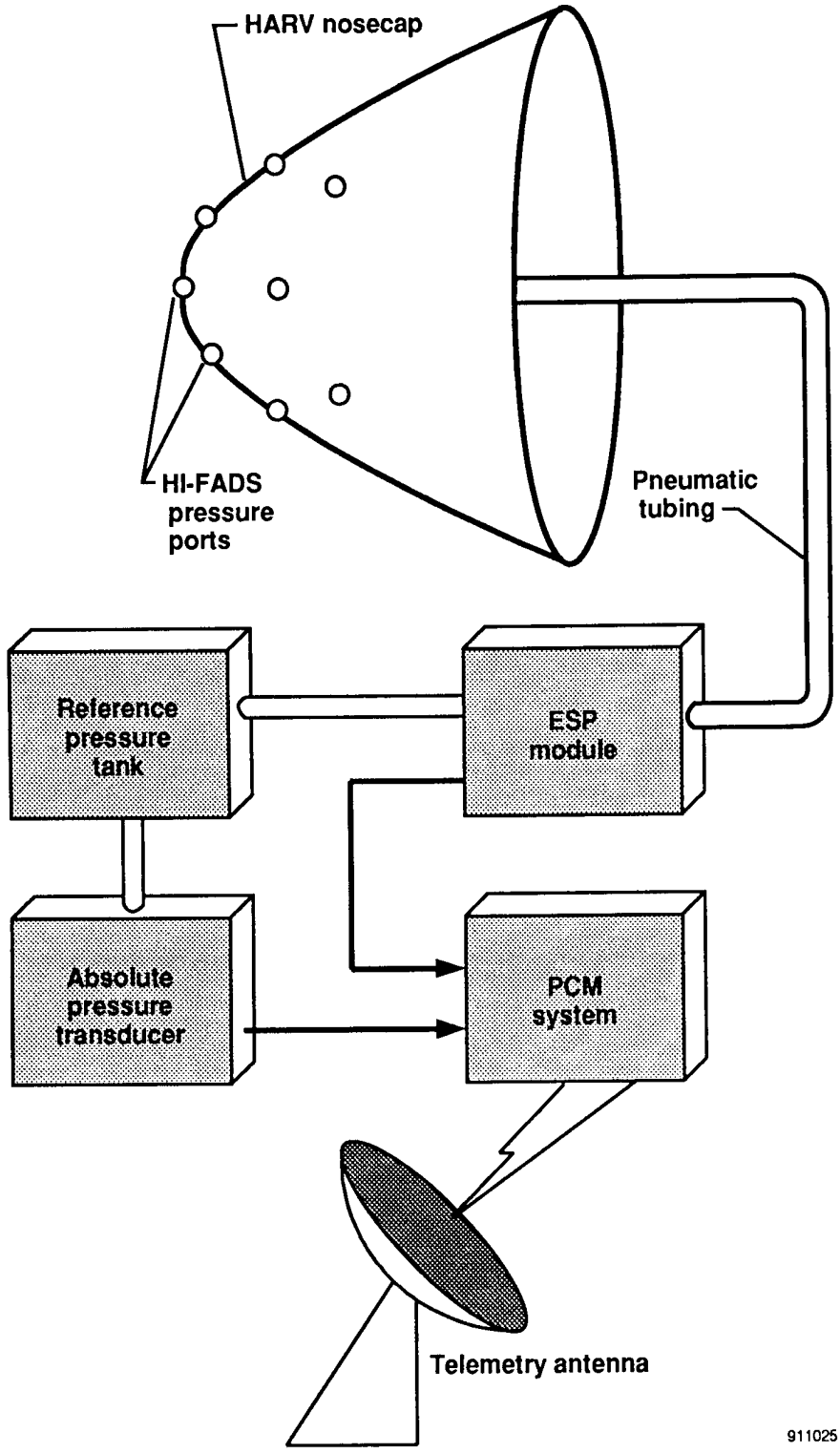


Figure 2. HI-FADS system hardward.

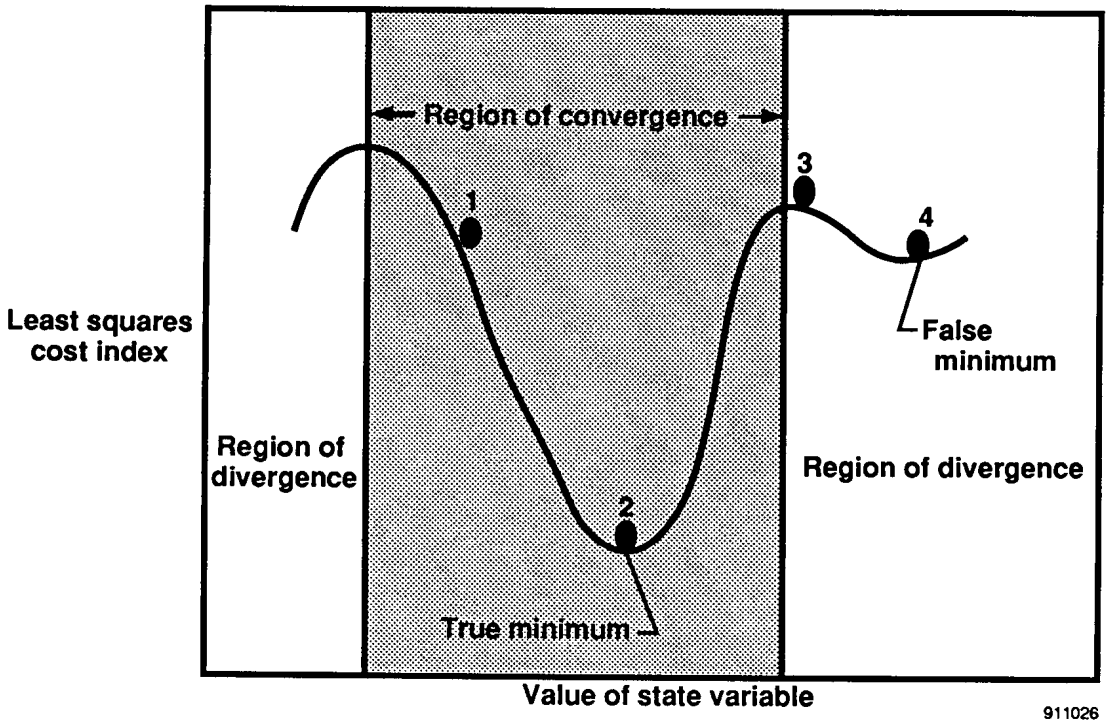


Figure 3. One-dimensional illustration of HI-FADS algorithm convergence and divergence regions.

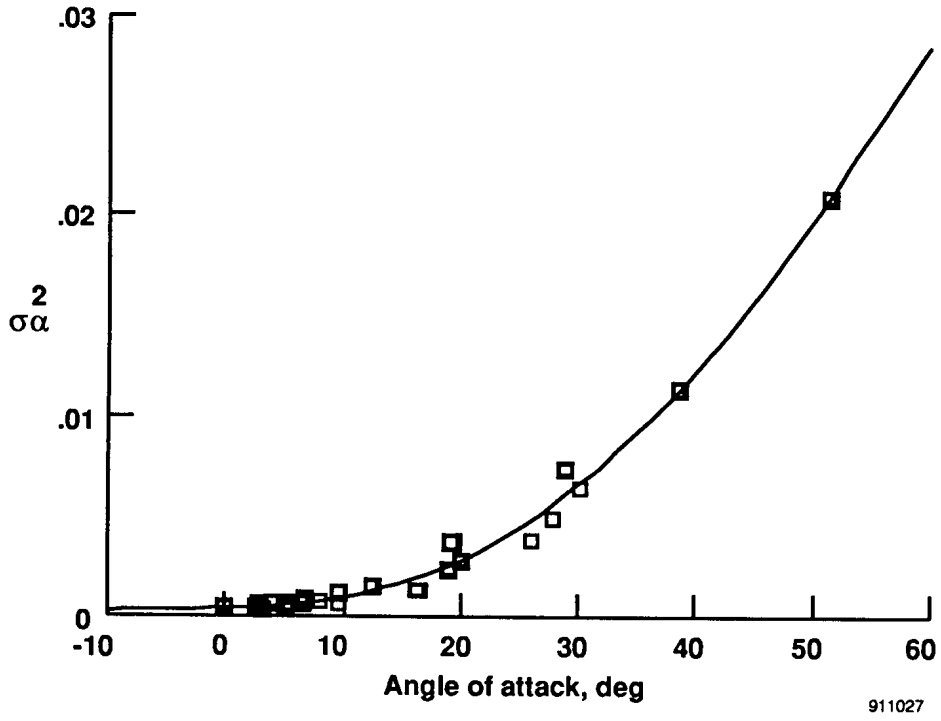


Figure 4. HI-FADS pressure residual variance as a function of angle of attack.

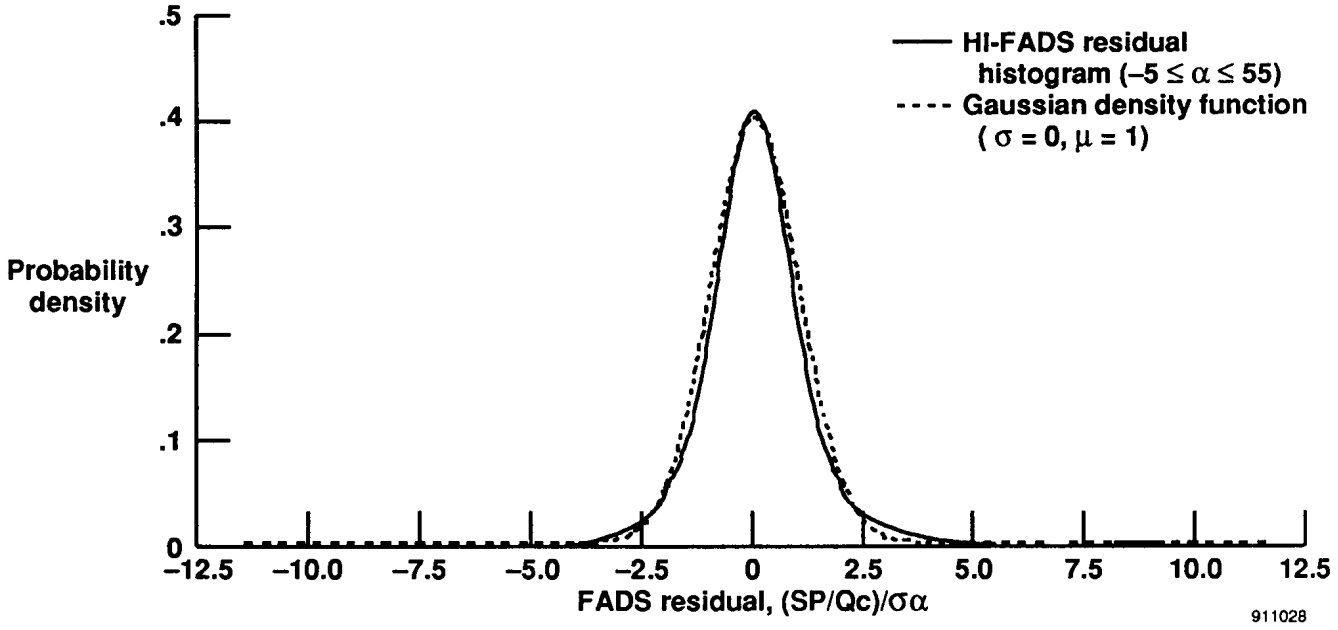


Figure 5. Normalized probability density for HI-FADS residuals

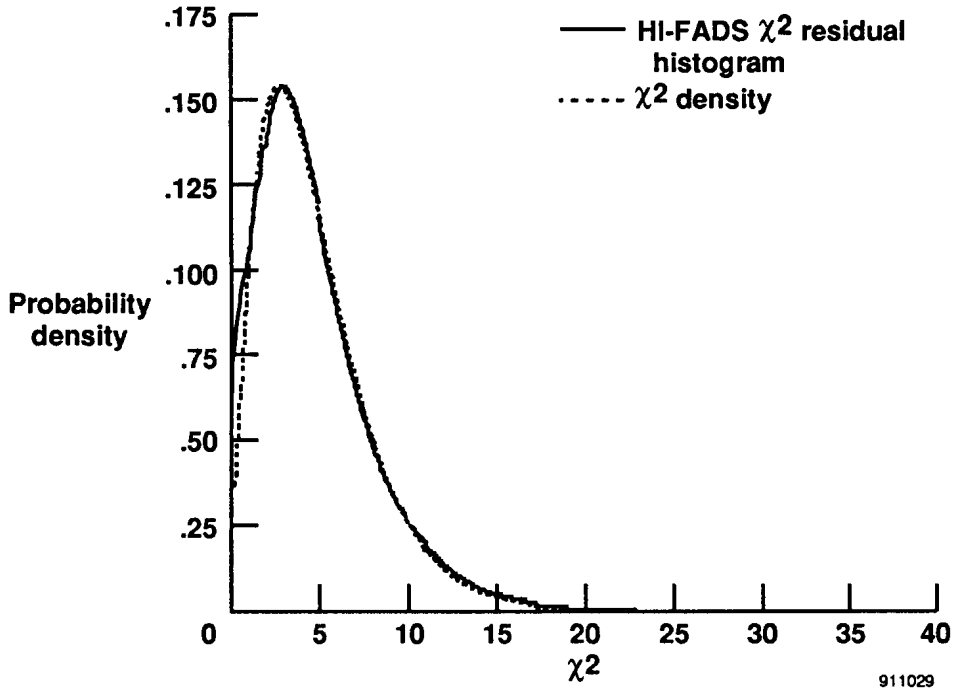


Figure 6. $\chi^2$ density for FADS residuals, 5-DOF.

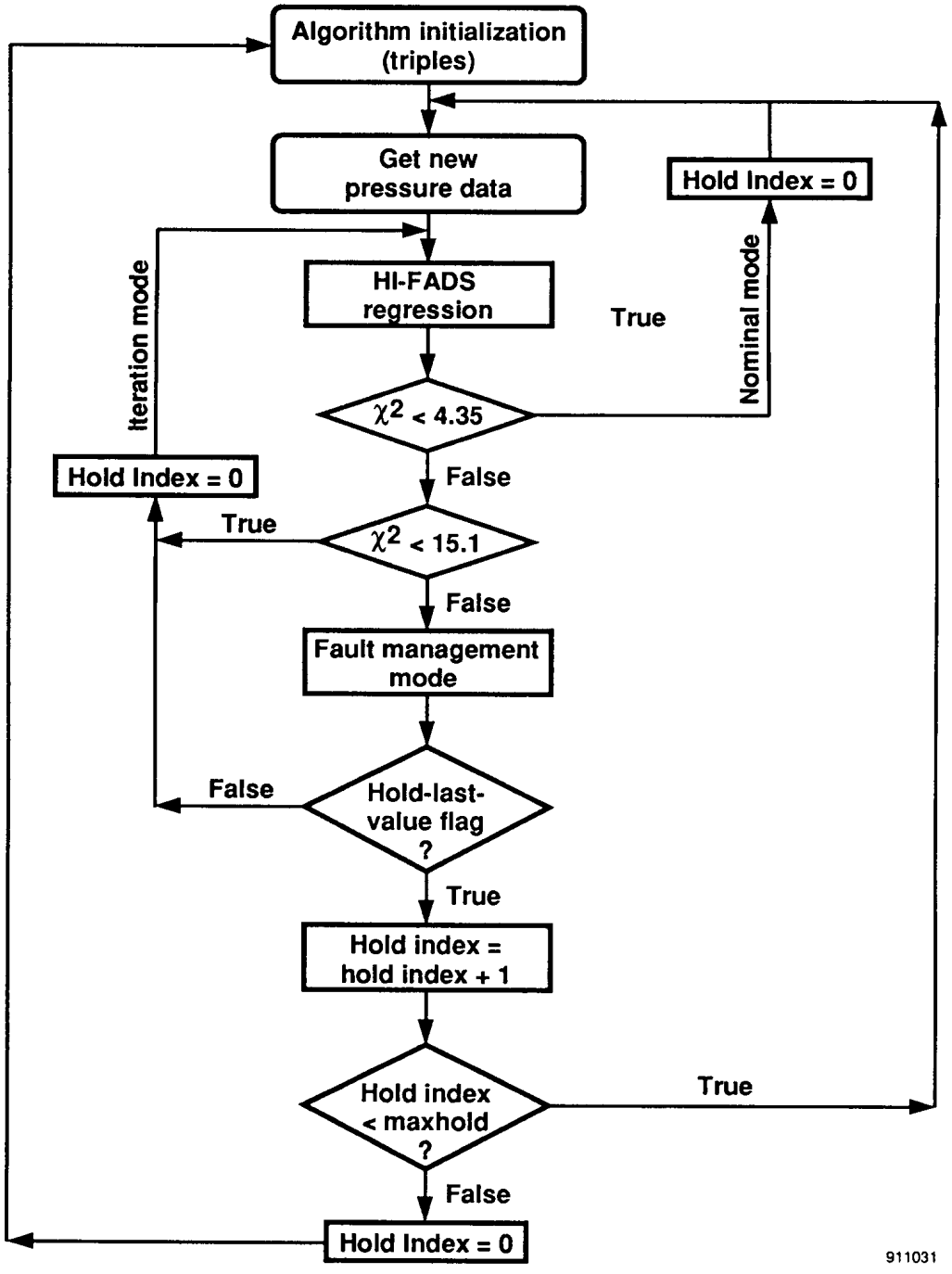


(a). Algorithm modes.

Figure 7. HI-FADS algorithm.

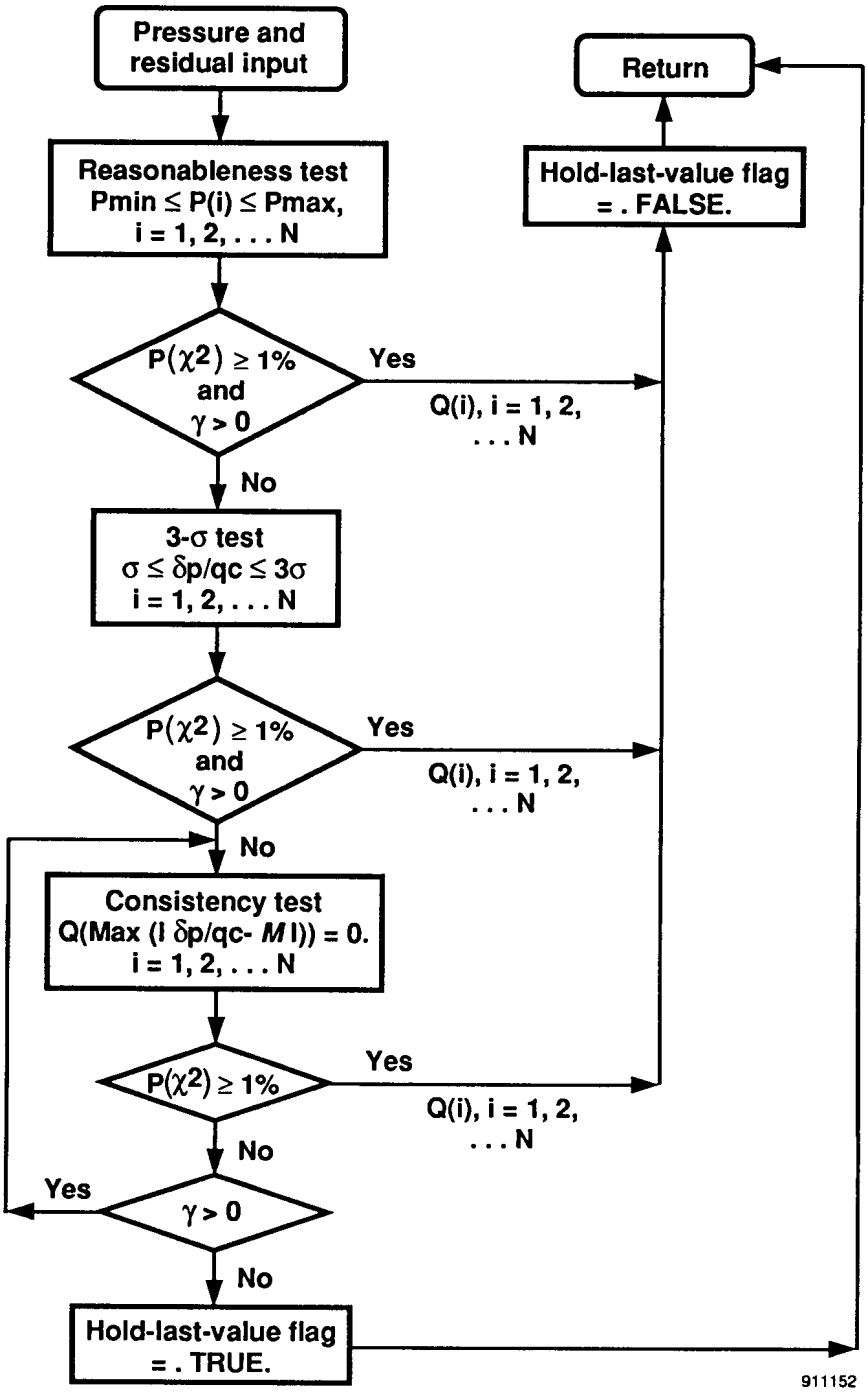


(b). Fault management mode.

Figure 7. Concluded.

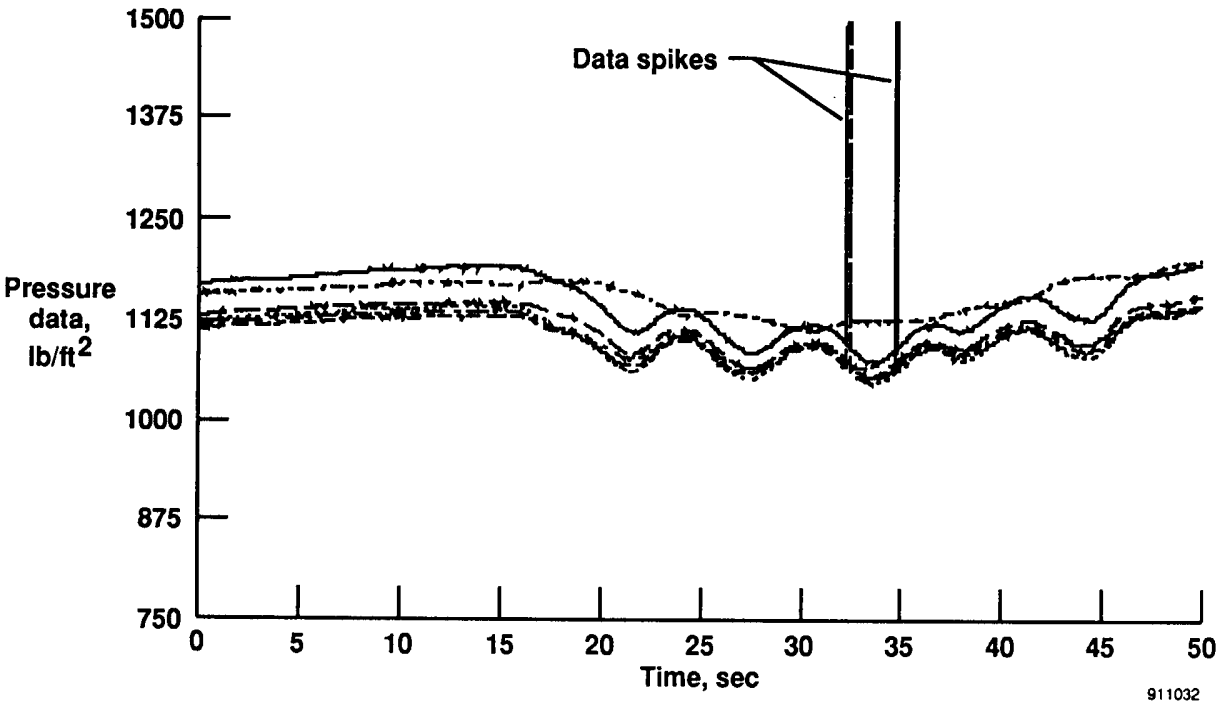


(a). Input pressure time history.

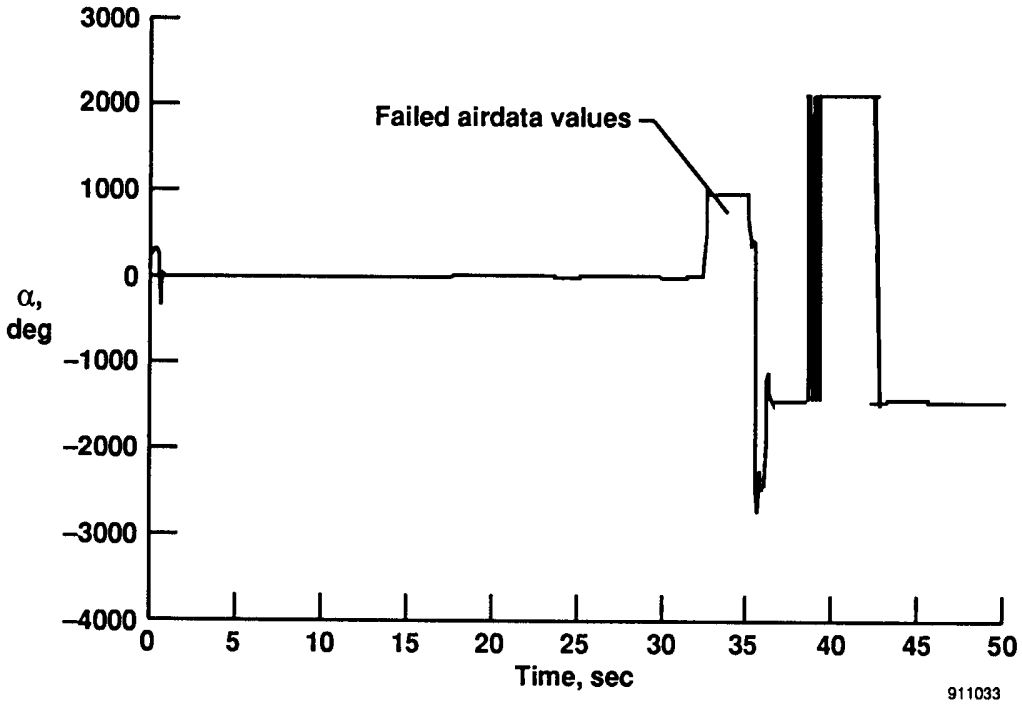


(b). HI-FADS angle-of-attack time history, no divergence protection.

Figure 8. HI-FADS computations performed in presence of data spikes.

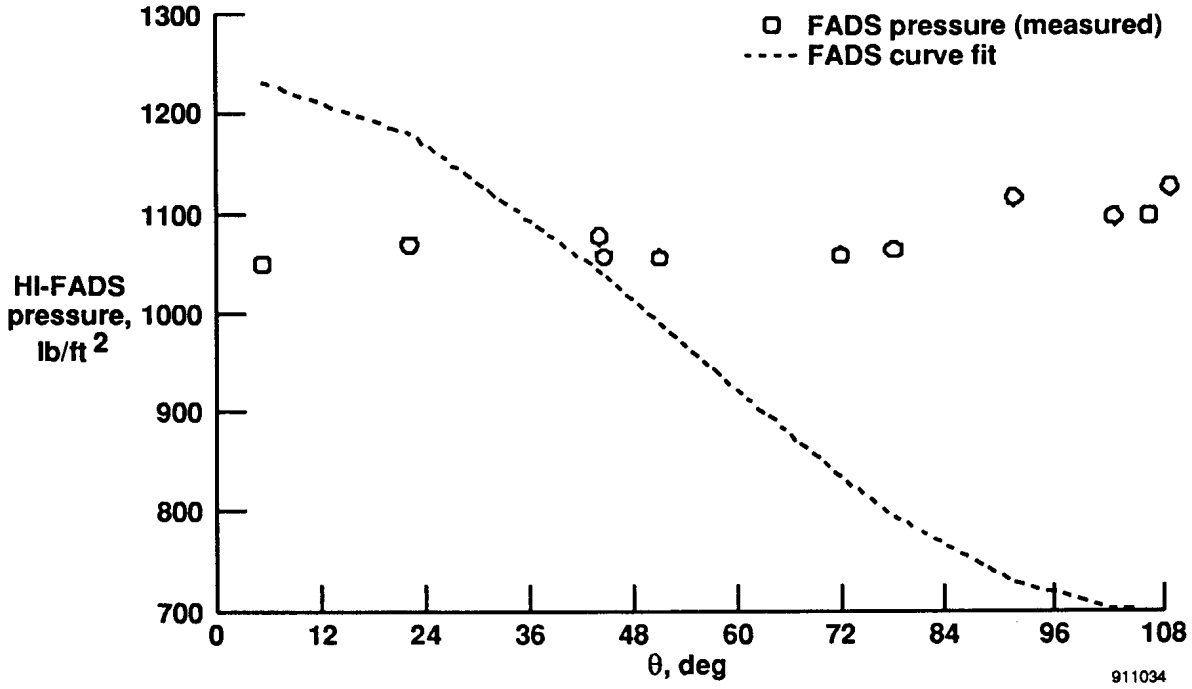


(c). HI-FADS curve fit for diverged airdata, $\chi^2 = 3750$.

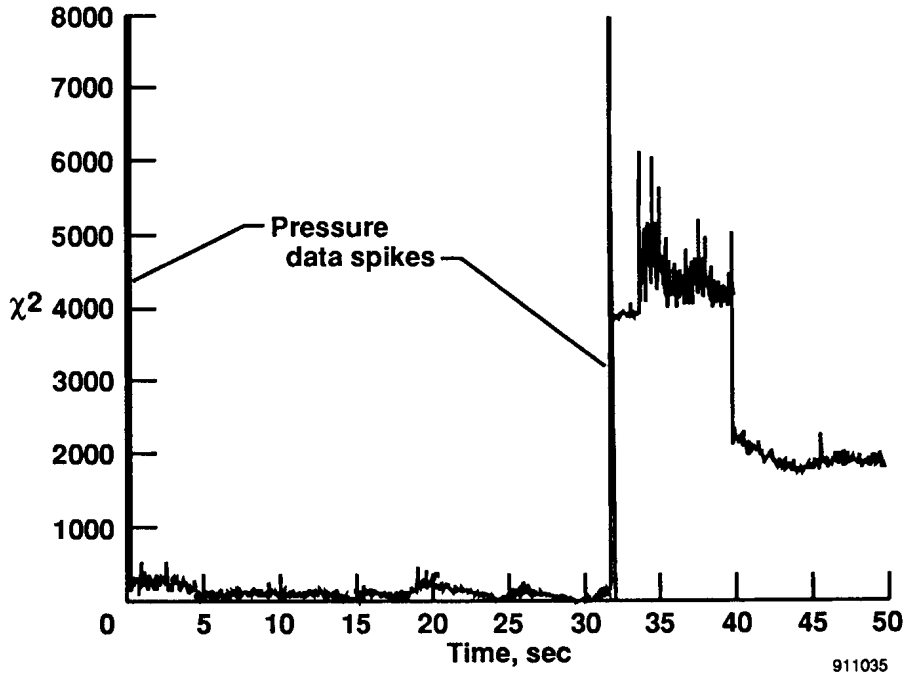


(d). $\chi^2$ time history, no divergence protection.

Figure 8. Continued.

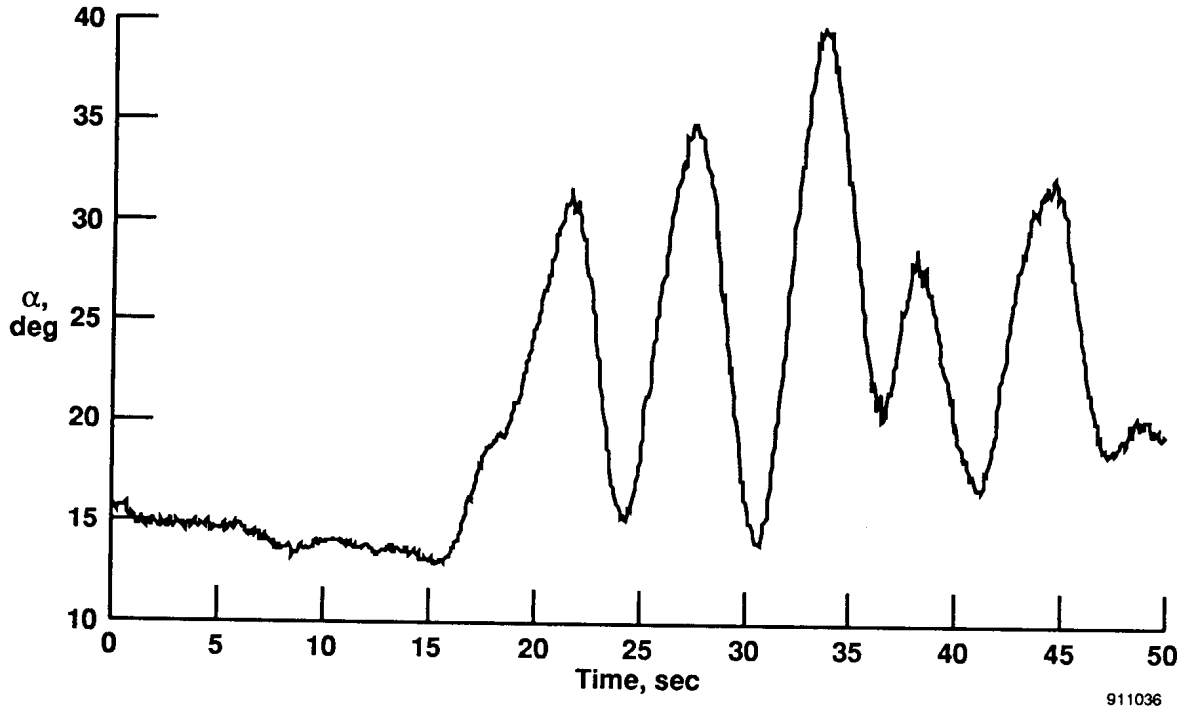


(e). HI-FADS angle-of-attack time history, divergence protected.

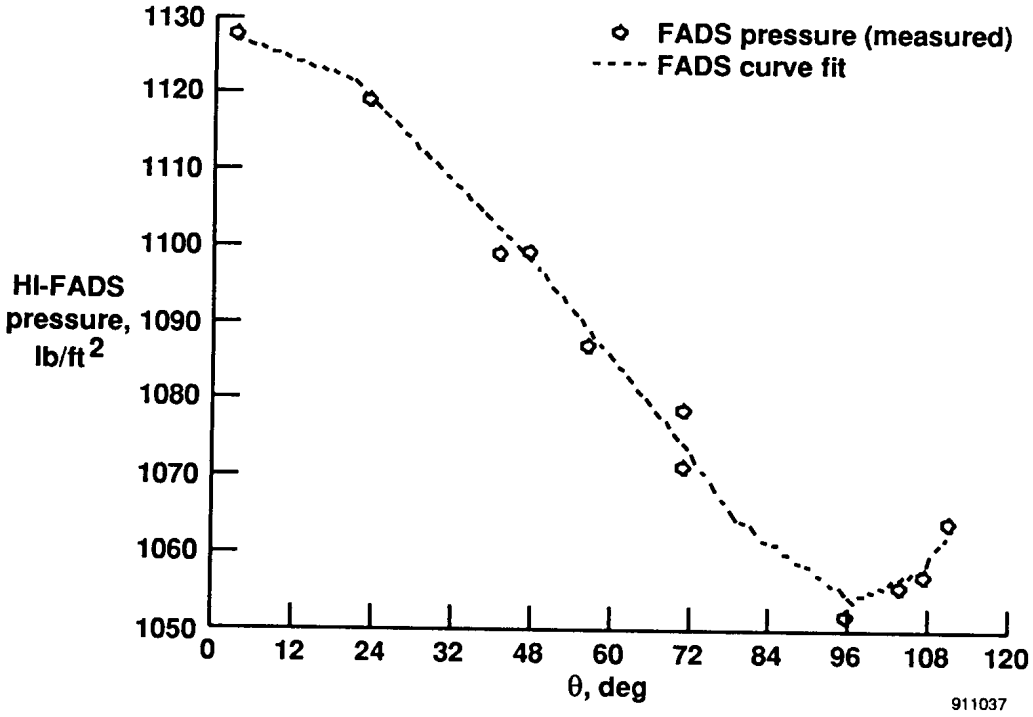


(f). HI-FADS curve fit for converged data, $\chi^2 = 3.45$.

Figure 8. Continued.

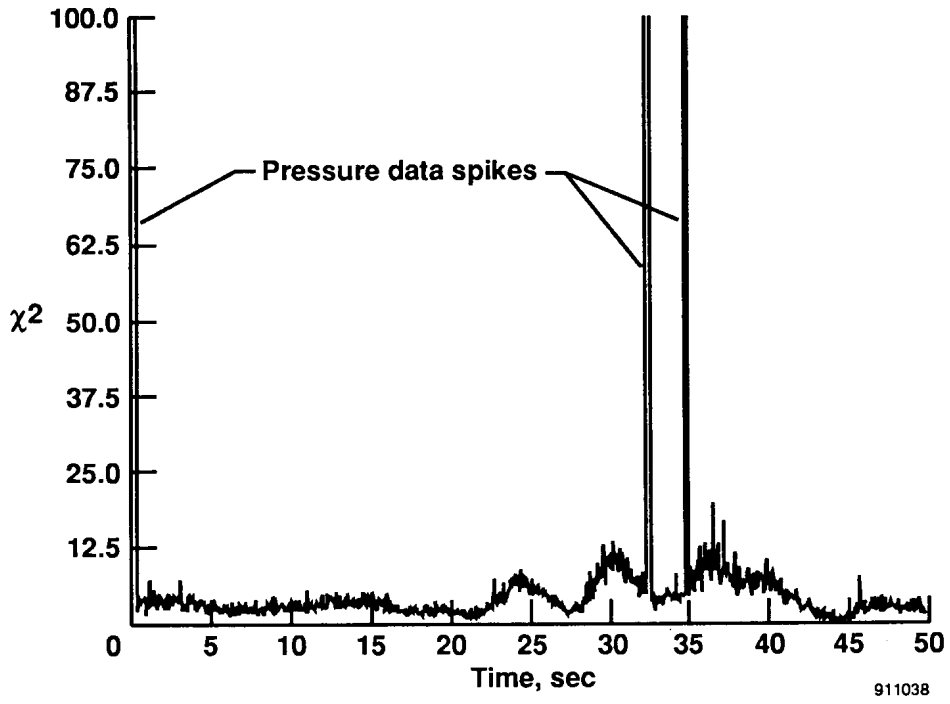


(g). $\chi^2$ time history, divergence protected.

Figure 8. Concluded.

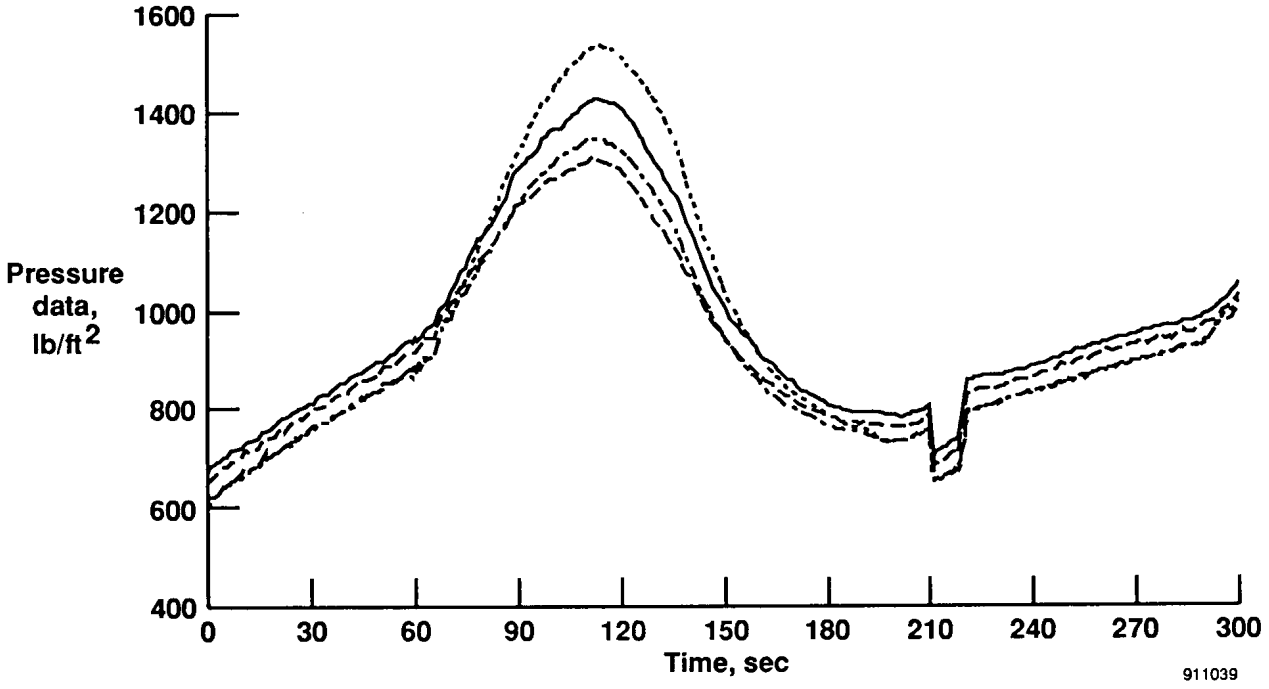


(a). Pressure input time history.

Figure 9. HI-FADS computations performed in presence of data steps.

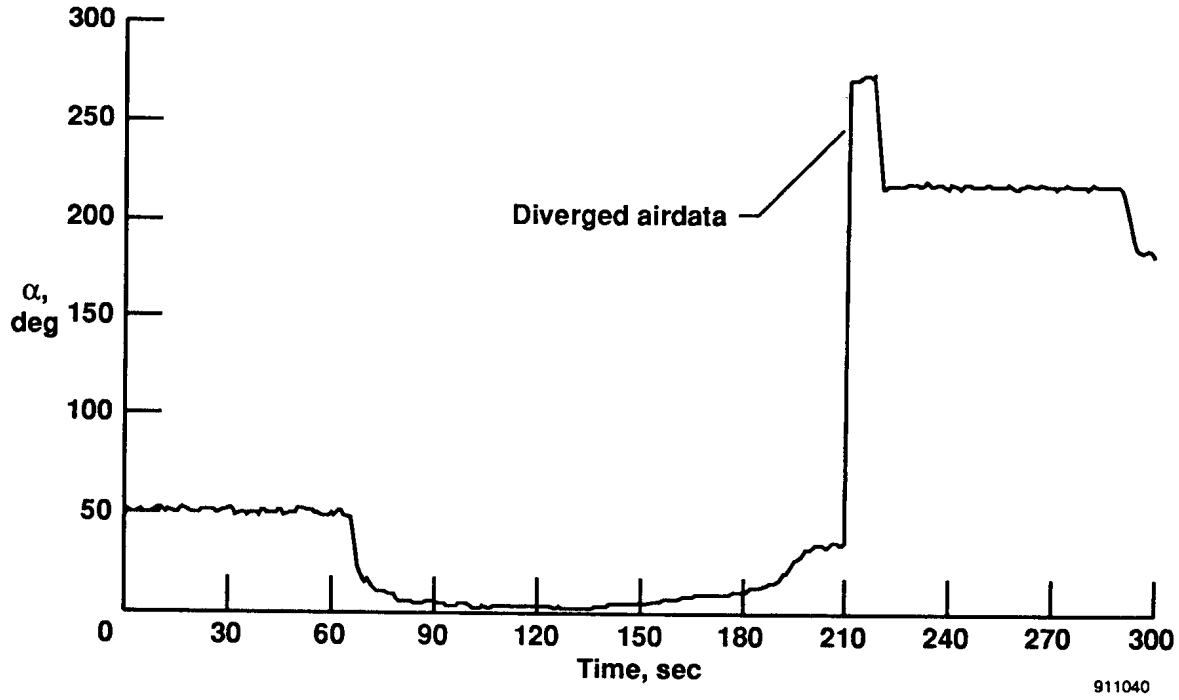


(b). HI-FADS angle of attack, no divergence protection.

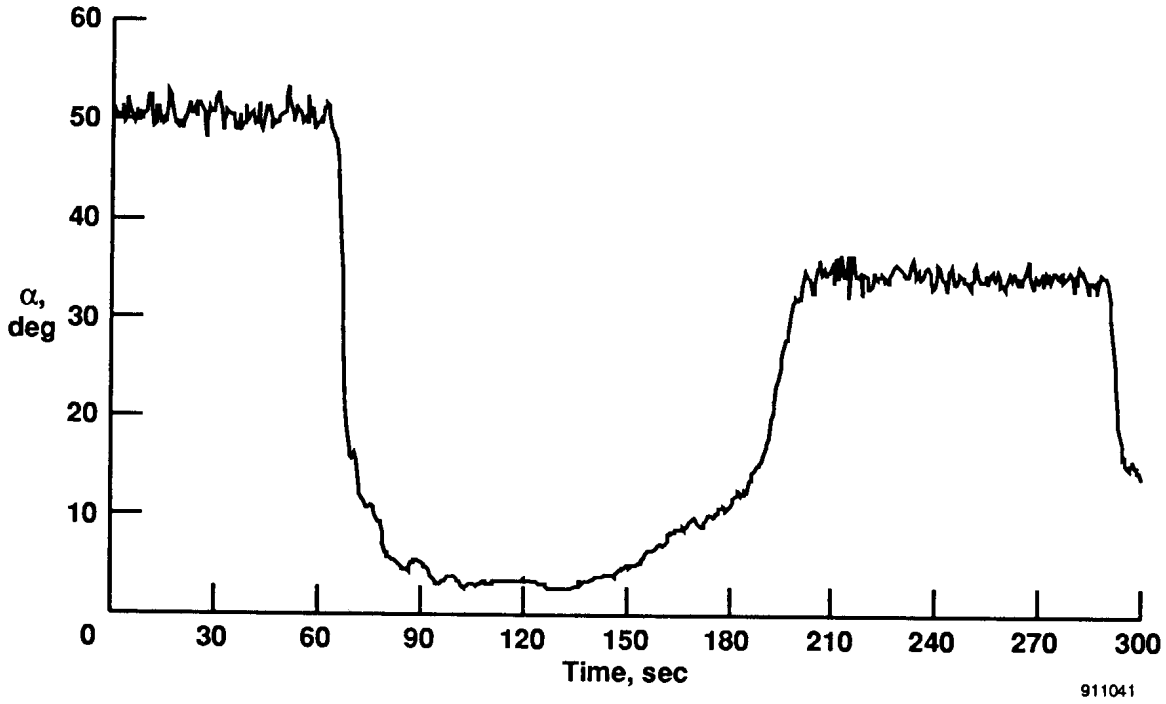


(c). HI-FADS angle of attack, divergence protected.

Figure 9. Continued.

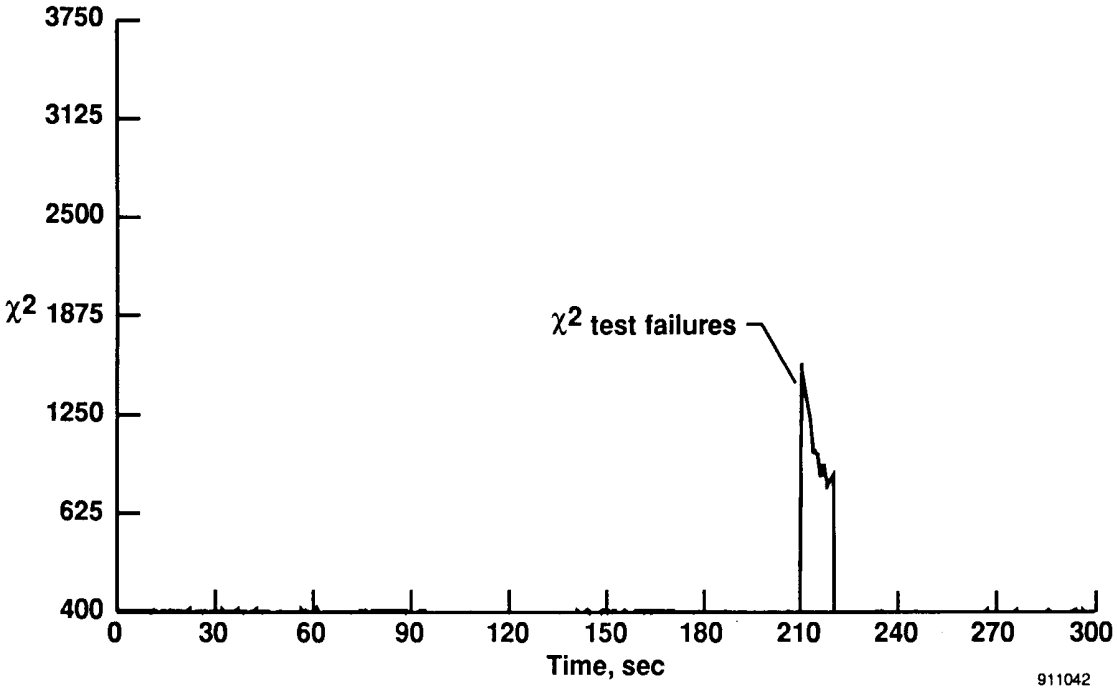


(d). $\chi^2$ time history, divergence protected.

Figure 9. Concluded.

# REPORT DOCUMENTATION PAGE

Form Approved
OMB No. 0704-0188



| 1. AGENCY USE ONLY *(Leave blank)* | 2. REPORT DATE | 3. REPORT TYPE AND DATES COVERED |
|---|---|---|
| | January 1992 | Technical Memorandum |

**4. TITLE AND SUBTITLE**

Failure Detection and Fault Management Techniques for a Pneumatic High-Angle-of-Attack Flush Airdata Sensing (HI-FADS) System

**5. FUNDING NUMBERS**

RTOP 505-68-40

**6. AUTHOR(S)**

Stephen A. Whitmore and Timothy R. Moes

**7. PERFORMING ORGANIZATION NAME(S) AND ADDRESS(ES)**

NASA Dryden Flight Research Facility
P.O. Box 273
Edwards, California 93523-0273

**8. PERFORMING ORGANIZATION REPORT NUMBER**

H-1780

**9. SPONSORING/MONITORING AGENCY NAME(S) AND ADDRESS(ES)**

National Aeronautics and Space Administration
Washington, DC 20546-0001

**10. SPONSORING/MONITORING AGENCY REPORT NUMBER**

NASA TM-4335

**11. SUPPLEMENTARY NOTES**

Presented as paper 92-0263 at the Aerospace Sciences Meeting, Reno, NV, January 6-9, 1992, American Institute of Aeronautics and Astronautics, Inc., (AIAA).

**12a. DISTRIBUTION/AVAILABILITY STATEMENT**

Unclassified — Unlimited
Subject Category 06

**12b. DISTRIBUTION CODE**

**13. ABSTRACT** ***(Maximum 200 words)***

A high-angle-of-attack flush airdata sensing system was installed and flight tested on the F-18 High Alpha Research Vehicle at the NASA Dryden Flight Research Facility. This system uses a matrix of pressure orifices arranged in concentric circles on the nose of the vehicle to determine angles of attack, angles of sideslip, dynamic pressure, and static pressure as well as other airdata parameters of interest. Results presented use an arrangement of 11 data ports distributed symmetrically on the aircraft nose.

Experience with this sensing system data indicates that the primary concern for real-time implementation is the detection and management of overall system and individual pressure sensor failures. The multiple port sensing system is more tolerant to small disturbances in the measured pressure data than conventional probe-based intrusive airdata systems. However, under adverse circumstances, large undetected failures in individual pressure ports can result in algorithm divergence and catastrophic failure of the entire system.

This paper demonstrates how system and individual port failures may be detected using $\chi^2$ analysis. Once identified, the effects of failures are eliminated using weighted least squares. Background on the HI-FADS hardware, the aerodynamic model, the nonlinear regression algorithm, and $\chi^2$ analysis are presented. Failure detection and fault management techniques are developed and data obtained from the High Alpha Research Vehicle flight tests are used to demonstrate the techniques.

**14. SUBJECT TERMS**

Airdata; Nonintrusive airdata; Fault tolerance; Pressure sensing; Chi square analysis

**15. NUMBER OF PAGES**

20

**16. PRICE CODE**

A03

| 17. SECURITY CLASSIFICATION OF REPORT | 18. SECURITY CLASSIFICATION OF THIS PAGE | 19. SECURITY CLASSIFICATION OF ABSTRACT | 20. LIMITATION OF ABSTRACT |
|---|---|---|---|
| Unclassified | Unclassified | Unclassified | Unlimited |